Charge Recombination in Phosphorescent Organic Light-Emitting Diode Host-Guest Systems through QM/MM Simulations

Tianyu Zhu and Troy Van Voorhis*

Department of Chemistry, Massachusetts Institute of Technology, 77 Massachusetts Avenue, Cambridge, Massachusetts 02139, United States

E-mail: tvan@mit.edu

Abstract

Host-guest systems are crucial for achieving high efficiency in most organic light-emitting diode (OLED) devices. However, charge recombination in such systems is poorly understood due to complicated molecular environment, making the rational design of host-guest systems difficult. In this article, we present a computational study of a phosphorescent OLED with 2,8-bis(triphenylsilyl)dibenzofuran (BTDF) as the host and *fac*-tris(2-phenylpyridine) iridium (*fac*-Ir(ppy)$_3$) as the guest, using a combined quantum mechanics/molecular mechanics (QM/MM) scheme. A new reaction coordinate is introduced to measure the electrostatic interactions between the host and guest molecules. Ionization potentials and electron affinities of the host show broader distributions as the host-guest interaction increases. Based on these distributions, we describe a molecular picture of charge recombination on the guest and find a direct charge trapping route for this system. Our results suggest several strategies for the design of more efficient host and guest combinations.

Introduction

Organic light-emitting diodes (OLEDs) have attracted significant attention for broad applications in displays and lighting because of their high electroluminescence (EL) efficiency, flexibility and low manufacturing cost.[1–6] In order to improve the EL efficiency, various fluorescent and phosphorescent materials have been introduced as OLED emitters.[3,7–9] In practice, it is phosphorescent OLEDs (PhOLEDs) that are utilized to obtain high external quantum efficiency (EQE) over 20%.[10–13] Because the ratio of singlet and triplet excitons under electrical excitation is 1:3 due to spin statistics,[14–16] the internal quantum efficiency (IQE) of traditional fluorescent OLEDs is limited to 25%. PhOLEDs, on the other hand, can achieve 100% IQE by harvesting both singlet and triplet excitons through strong spin-orbit coupling.[17–20]

Nearly all PhOLEDs are based on the host-guest systems in which triplet emitters are

dispersed homogeneously into host materials, constituting the emission layer in PhOLED devices, in order to minimize triplet-triplet annihilation and triplet exciton quenching.[21–23] It is shown in numerous experimental studies that the EQE of PhOLEDs is significantly affected by the combination of host and guest.[24–28] For instance, Chen and coworkers[24] reported that the maximum EQE for FIrpic doped in SimCP *vs.* mCP is 14.4% *vs.* 12.3%, while a different dopant FIrN4 in combination with the same two hosts gives the maximum EQE of only 9.4% and 5.8% respectively. Therefore, to design more efficient OLED devices, it is crucial to understand how different host-guest combinations influence the charge transfer and charge recombination processes in the emission layer.

Nevertheless, comparatively little is known about how charge recombination works in host-guest systems. Several competing mechanisms have been proposed for the charge recombination. First, electrons and holes can directly combine on the guest, which causes the formation of excitons and thereafter guest emission.[29,30] However, it is not clear whether or not an electron and a hole are transported simultaneously to the guest. One charge carrier might be trapped on the guest in advance, attracting a charge of opposite sign to form an exciton. Second, excitons can be formed primarily on the host and then transfer their energies to the guest via Förster[31] or Dexter[32] mechanisms. Besides, a third possibility is that excitons can also be formed on the closest host-guest pairs. The direct charge recombination on the guest requires the offset of HOMO and LUMO energy levels between the host and the guest, while the host to guest energy transfer needs spectrum overlap (Förster)[33] or wavefunction overlap (Dexter)[32] between the donor and the acceptor.

In this article, we simulate a model PhOLED emission layer, in which the organometallic complex *fac*-tris(2-phenylpyridine) iridium (*fac*-Ir(ppy)$_3$) and 2,8-bis(triphenylsilyl) dibenzofuran (BTDF) are chosen as the guest and host, structures shown in Figure 1. Ir(ppy)$_3$ is a well-known green phosphorescent emitter reported to achieve a maximum EQE over 20%,[10,11,34,35] which makes it a good candidate for full color displays. BTDF is an electron-conducting host designed for hole-conducting deep-blue emitters where the maximum EQE

of such OLEDs are above 17%.[36] Andrienko and coworkers did a number of computational studies on the morphology and charge transfer properties of BTDF-hosted PhOLEDs on various length scales.[37,38]

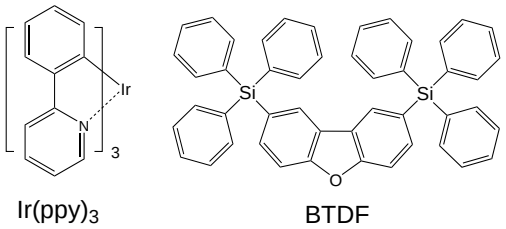

Figure 1: Molecular structures of $Ir(ppy)_3$ and BTDF.

While several theoretical methods exist for treating charge transfer problems in organic optoelectronics,[39,40] we use a combined quantum mechanics/molecular mechanics (QM/MM) approach[41–43] and obtain a molecular picture of the charge recombination process for this $Ir(ppy)_3$/BTDF model system. We are particularly focusing on one step – charge recombination from host to guest, among many other important steps for PhOLEDs. We find that the ionization potential (IP) and electron affinity (EA) of the host are distributed more widely near the guest. Such broader distribution slows down the electron transfer from host to guest. Contrarily, holes are injected into the guest in a barrierless fashion, after which electrons can be transferred faster to the guest due to the attraction from on-site holes, to create excitons. Our results reveal that one possible charge recombination mechanism in this model is direct charge trapping but not very well balanced. Based on these results, this work provides suggestions for rational design of good host and guest combinations in PhOLEDs.

Computational Methods

We began our study on the $Ir(ppy)_3$/BTDF system with a molecular dynamics (MD) simulation, where the simulation box contained 15 $Ir(ppy)_3$ and 250 BTDF molecules that were treated classically (Figure 2, left panel). We set the guest to host mass ratio to be approximately 6% to match the experimental values of $Ir(ppy)_3$-doped systems (3%-10%).[10,34,35]

From the MD trajectory, we extracted snapshots and then performed a large number of polarizable QM/MM (pol-QM/MM) single-point calculations on the cation, anion and neutral states of the guest and the host, in order to obtain IPs and EAs of both species. For each snapshot, a host or a guest molecule was chosen as the QM region (Figure 2, right panel), while all the other molecules were described by MM force fields. In addition, as we found the hole transfer from the host to the guest is thermodynamically downhill while the electron transfer is mostly uphill, we also wanted to investigate the electron transfer from the host to the positively-charged guest and the formation of excitons on the guest. Thus, we also performed excited state pol-QM/MM calculations. The details of MD and QM/MM simulations are described below.

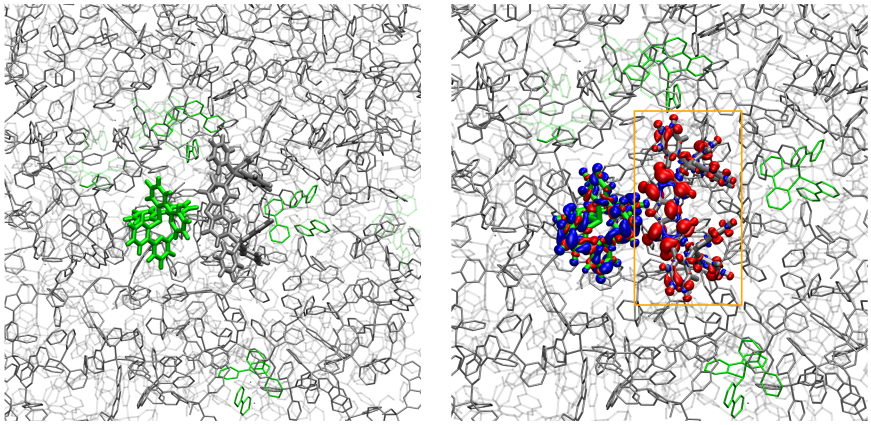

Figure 2: Illustration of the QM/MM method. Left: Disordered cell of the $Ir(ppy)_3$(green)/ BTDF(gray) system generated by MD simulation. Right: Selection of a BTDF anion as the QM region for calculation of the BTDF electron affinity near an $Ir(ppy)_3$ cation.

MD Simulation. To start the MD simulation, the host and guest molecules were inserted randomly into a simulation box as the initial configuration using PACKMOL package.[44] We annealed the system from 0K to 500K during 2ns and then simulated the system at 500K in an NPT ensemble for another 2ns to make sure the equilibrium density was reached. The host-guest system was equilibrated at the high temperature (500K) so that the molecules became uncorrelated in space and well-sampled amorphous structures can be obtained. The

system was then cooled to the room temperature (300K) during 1ns, after which a 3ns simulation in NPT ensemble at 300K was performed. The final 2ns of the NPT dynamics was sampled at 0.2ns intervals to obtain 10 snapshots for QM/MM calculations. All MD simulations were carried out using GROMACS 4.5.5 package[45] and OPLS force field.[36,46] The MD simulation parameters can be found in Supporting Information.

QM/MM Calculations. All of the QM/MM calculations were done using the CHARMM[47]-QChem[48] interface.[49] All density functional theory (DFT) calculations for QM regions were performed with QChem 4.1 package using the PBE0 functional[50] and 6-31G* basis set[51] for BTDF and LANL2DZ[52] effective core potential basis set for $Ir(ppy)_3$. All of the excited state calculations were done using a restricted open-shell Kohn-Sham (ROKS) approach.[53] ROKS calculates the lowest singlet excited state (S_1) energy by optimizing the KS orbitals to minimize a linear combination of single-determinant energies.

The QM/MM method must take the polarizable organic semiconductor environment into account apart from the electrostatic effects. Therefore, we introduced fictitious "drude" charges in our pol-QM/MM method that are harmonically attached to MM charges.[54] These classical drude particles are allowed to respond instantaneously to the electric fields and correspondingly move to their local energy minima positions. The induced polarization can thus be simulated through such simple treatment. The drude charge parameters were fitted to reproduce the polarizability of the host and guest computed employing DFT (see Supporting Information).

With pol-QM/MM computed energies, we calculated IPs and EAs of the host and guest using the ΔSCF method:

$$IP = E_+ - E_0 \quad (1)$$

$$EA = E_0 - E_- \quad (2)$$

where E_+, E_-, E_0 are the energies for cation, anion and neutral states.

We performed pol-QM/MM calculations on all 250 host molecules and 15 guest molecules from the MD simulation box. The QM region is either a host or a guest molecule. To make the sampling representative enough, we did calculations for 2 snapshots of 250 host molecules and 10 snapshots of 15 guest molecules.

Reaction Coordinate. To understand the charge recombination in a host-guest system, it is significant to know the hole and electron energy levels of the host in different molecular environment, i.e., bulk phase and near the guest. Since the guest is doped into the host at a small ratio, it can be assumed that the charges are first transferred to the host which is far away from the guest (similar to bulk phase) and then to the host near the guest and finally to the guest. Thus, we need a definition for the "distance" between the host and guest. However, distance between molecules is poorly defined in such system because the molecules are about the similar size ($\sim$1 nm) as the space between their centers of mass (1-5 nm). Besides, as there are many guest molecules in the simulation box, it is ambiguous to determine which host-guest distance to use for a specific host.

In this study, we introduce a new reaction coordinate — the "host-guest interaction energy", to evaluate the influence of the guest on the host energy levels. Since the electrostatic energy between two molecules is inversely proportional to their distance, this energy can be used to indirectly measure the distance. To avoid the ambiguity of choosing specific host-guest electrostatic energy, we evaluate the electrostatic effects of all guests on one host by calculating its IP/EA under two different electrostatic environments. Therefore, we define the host-guest interaction energy as the difference of two sets of the host IP/EA. The three steps to obtain the host-guest interaction energy are:

1. Calculate the IP/EA (marked as IP(on)/EA(on)) of the host molecules.

2. Turn off all MM and drude charges on all guests, then re-calculate the IP/EA (IP(off)/EA(off)) of the same set of host.

3. The host-guest interaction energy is given by:

$$|\Delta IP| = |IP(off) - IP(on)| \quad (3)$$

$$|\Delta EA| = |EA(off) - EA(on)| \quad (4)$$

Using the difference of IP or EA values due to the existence/absence of the guest charges, we find a better way to describe the electrostatic and polarizable effects on the host energetics caused by the guest.

Results

We first show electron affinities and ionization potentials of the host as a function of the host-guest interaction energy in Figures 3-4. Eq. 4 was employed to compute the host-guest interaction energy as the reaction coordinate for EA, while for IP we used Eq. 3. In experiments, −IP and −EA of solid materials are usually measured relative to the reference energy levels using ultraviolet photoemission spectroscopy (UPS) and inverse photoemission spectroscopy (IPES).[55,56] In some literatures, −IP and −EA are called the highest occupied molecular orbital (HOMO)/lowest unoccupied molecular orbital (LUMO) energies, though which is not strictly accurate. Here, we plot −IP and −EA to be consistent with the experiments.

Clearly there is much scatter in the data (Figures 3-4), although there is also a trend. To be quantitative about the scatter and trend of EA as a function of the distance from the guest, we need to use the data to estimate both the average value of EA at a given point on the reaction coordinate and also its standard deviation. For this purpose we use the kernel density estimation (KDE), a statistical tool for reconstructing probability distributions from scattered data.[57,58] We use a small Gaussian distribution (the kernel) centered on each data point to simulate its probability. The overall probability distribution of EA is thus given by

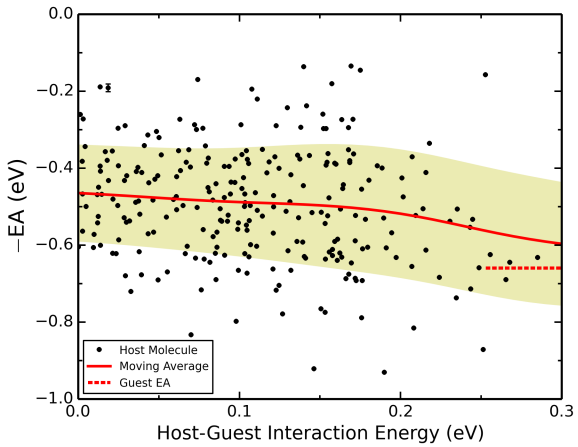

Figure 3: Electron affinities of the host as a function of the host-guest interaction energy $|\Delta EA|$. The yellow region covers the moving average plus/minus the moving standard deviation ($\overline{EA} \pm \sigma_{EA}$). The error bar is shown for one data point (0.0188, -0.1913).

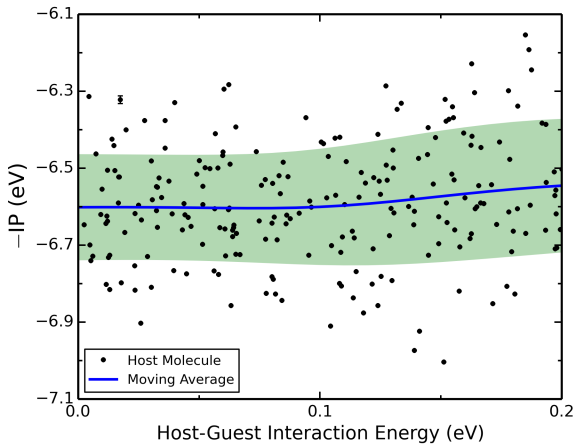

Figure 4: Ionization potentials of the host as a function of the host-guest interaction energy $|\Delta IP|$. The green region covers the moving average plus/minus the moving standard deviation ($\overline{IP} \pm \sigma_{IP}$). The guest IP (5.10eV) is not shown as it is much higher than the host IP. The error bar is shown for one data point (0.0175, -6.3222).

Eq. 5, where $|\Delta EA|_i$ is each data point's value of $|\Delta EA|$, N is the number of data points and α is the coefficient of the Gaussian distribution. We choose $\alpha = 300$ so that the probability estimation is close to the true probability while the probability curve is kept smooth. The average and the standard deviation of EA are given by Eq. 6-7, where EA_i is each point's value of EA. For IP, the same equations are used but EA data are replaced by IP data.

$$\rho(|\Delta EA|) = \frac{1}{N}\sqrt{\frac{\alpha}{\pi}}\sum_{i=1}^{N} e^{-\alpha(|\Delta EA|-|\Delta EA|_i)^2} \quad (5)$$

$$\overline{EA}(|\Delta EA|) = \frac{\frac{1}{N}\sqrt{\frac{\alpha}{\pi}}\sum_{i=1}^{N} EA_i \cdot e^{-\alpha(|\Delta EA|-|\Delta EA|_i)^2}}{\rho(|\Delta EA|)} \quad (6)$$

$$\sigma(|\Delta EA|) = \sqrt{\frac{\frac{1}{N}\sqrt{\frac{\alpha}{\pi}}\sum_{i=1}^{N}(EA_i - \overline{EA}(|\Delta EA|))^2 \cdot e^{-\alpha(|\Delta EA|-|\Delta EA|_i)^2}}{\rho(|\Delta EA|)}} \quad (7)$$

Through this KDE procedure, we obtain a smooth moving average curve, which is very useful to describe the IP/EA trend at different distance. Meanwhile, the standard deviation provides a quantitative view of the broadness of the data distribution. It can be seen in Figure 3 that the host $-\overline{EA}$ becomes a little lower as the host-guest interaction energy increases. Note that when the host-guest interaction energy is large, the host molecule is close to a guest. The fact that the change of moving average is not much indicates that the host-guest distance is not a key factor for changing host EA values. More importantly, as shown from the scatter plot and the standard deviation (σ_{EA}), the distribution of the host EA is broader as the host gets nearer the guest. We have also used ΔEA as the reaction coordinate to explain this distribution change, see Figure S1. This change has an effect on the electron transfer from the host to the guest. When the host is far from the guest, $-\overline{EA} \pm \sigma_{EA}$ is higher than the guest $-EA$ (-0.66eV), which suggests that the electron transfer would mostly be thermodynamically downhill. However, as the host gets closer to the guest, the distribution of the host EA is approaching the guest EA. Finally, most of the host $-EA$ data are even lower than the guest $-EA$, causing the electron transfer to be much less efficient because the electron transfer becomes a uphill process.

Similar to electron affinities, ionization potentials of the host also show a wider distribution as the host-guest interaction increases, see Figure 4. However, this change does not affect the hole transfer from the host to the guest, because the guest $-IP$ (-5.10eV) is much higher than the host $-IP$ in spite of the broader distribution. Therefore, it is always

a thermodynamically downhill process for the hole transfer to the guest.

From our pol-QM/MM simulations, the averaged IPs/EAs of $Ir(ppy)_3$ and BTDF are 5.10eV/0.66eV and 6.60eV/0.47eV. The experimental values of the IP and EA are 5.1-5.3eV and 1.9eV for $Ir(ppy)_3$,[59,60] while for BTDF the IP and EA are 6.54eV and 1.68eV.[38] Our calculated IPs agree very well with the experiments, but the EAs are underestimated. Possible reasons may be that the basis sets used in DFT are not large enough or the drude particle parameters in QM/MM simulations are not accurate. It should also be considered that the experiments have errors, espcially for the measurement of EAs. To understand the basis set and functional effects on IP/EA data, we did a small batch of QM/MM calculations employing larger basis sets and different functionals (see Supporting Information for details). Although the larger basis set or some particular functional gives results which are closer to the experimental data, the IP/EA values of BTDF and $Ir(ppy)_3$ change in the same direction. The relative energy level relationship between the host and guest is not altered, so our conclusion about the charge recombination will not be affected. Thus, our basis sets and functional are sufficient for obtaining useful insights.

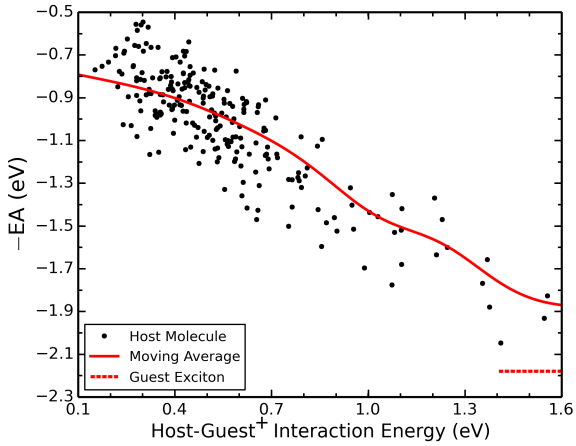

Figure 5: Electron affinities of the host near a guest cation as a function of the host-guest$^+$ interaction energy $|\Delta EA|$.

Since the driving force for the electron transfer step is uphill for many host-guest pairs, such a process cannot contribute significantly to efficient charge recombination on the guest.

In this paper, we would like to search for a recombination pathway where the reaction steps are all downhill. Transferring holes from host to guest first is the only candidate to achieve high recombination efficiency based on Figures 3-4. Therefore, it is reasonable to further consider the electron transfer from the host to the positively-charged guest. To obtain the host electron affinity near a guest cation, we performed pol-QM/MM calculations on all host molecules in one snapshot where one guest is positively charged, shown in Figure 5. Note that the QM region is still one host molecule while the environment has changed due to the existence of the guest cation. Instead of the host-guest interaction energy, we use the host-guest$^+$ interaction energy here as the reaction coordinate. The only difference is that EA(on) in Eq. 4 is now the host EA from the calculation with the existence of a guest cation. Because the electron transfer to a guest cation would induce the formation of an exciton, it is necessary to compute the guest exciton energy level to compare with the host EA. We did pol-QM/MM calculations on the guest utilizing the ROKS approach to obtain S_1 energy (E_{S_1}) and ($-IP + E_{S_1}$) was used as an estimation to the guest exciton energy level. As there are fewer data points, we choose $\alpha = 30$ for the KDE procedure here (Eqs. 5-7). As seen from Figure 5, there is a strong correlation between the host EA and the host-guest$^+$ interaction energy: $-EA$ becomes significantly lower when the interaction energy is larger. It is also observed that all host electron affinities are above the guest exciton energy level (-2.18eV), even for the ones that are very close to the guest. The electron transfer from the host to the guest cation becomes thermodynamically downhill due to the strong attraction of the guest holes. Therefore, this process completes the recombination pathway, and this is the only pathway that could possibly contribute to efficient electron-hole recombination directly on the guest.

Discussion

To understand the distribution in Figures 3-4, we relate the host-guest interaction to the host-guest distance and their relative orientations. In a pol-QM/MM calculation of E_+ and E_- of a host molecule, the dominant electrostatic interaction is charge-dipole interaction between the host and its surroundings, while for E_0 the dipole-dipole interaction dominates. Meanwhile, there are many possible relative molecular orientations between the host and guest, which results in a distribution of host EA and IP. When the host-guest interaction energy for a host molecule is large, at least one guest is close to the host. As a result, the molecular environment of this host is different from its bulk phase, as the guest has a distinct dipole moment from the host. In our model, $Ir(ppy)_3$ has a larger dipole (6.18D) than BTDF (0.87D) based on the DFT calculations. Therefore, the host near the guest has a broader distribution of EA and IP than in the bulk phase, as shown in Figures 3-4.

In Figure 5, a guest cation exists in the environment. Thus, the dominant electrostatic interaction between the host and guest becomes charge-charge interaction for E_- and dipole-charge interaction for E_0. Correspondingly, the EA distribution has a very strong correlation with the host-guest$^+$ interaction energy because the electrostatic interaction is much stronger than in Figures 3-4.

To better understand how charges recombine on the guest, we present Figure 6 and Figure 7 to explicitly describe the related processes. In Figure 6, we demonstrate the charge migration from the host to the guest through the direct charge trapping, while the electron transfer to the guest cation is shown in Figure 7. As shown in Figure 6, the charge migration to the guest can be divided into two steps: (1) from the bulk phase host to the host close to the guest; (2) from the nearby host to the guest. As the average EA and IP is similar between the host in the bulk phase (small host-guest interaction) and the host near the guest (large host-guest interaction), the first step is just as charge migration in the host material. However, the second step is different for the electron and hole transfer. For the electron transfer, as the host becomes closer to the guest, the host $-EA$ is slightly lower and its

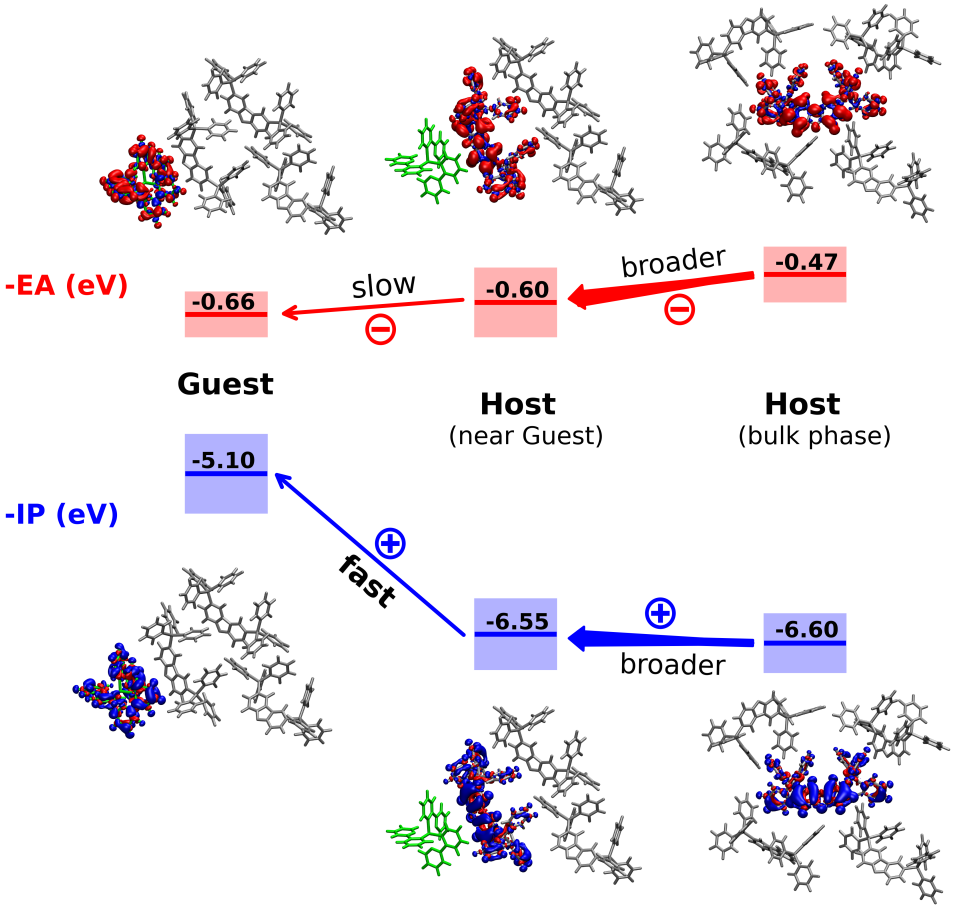

Figure 6: Charge recombination on the guest through direct electron and hole trapping. The standard deviations are shown by the blue/red regions around the energy levels.

distribution becomes broader. As a result, many electrons get trapped on the host whose $-EA$ is below that of the nearby guest. Therefore, the electron migration is not as fast as from the host bulk phase to the guest. On the other hand, the hole transfer remains fast as the host is approaching the guest, because it is impossible to trap holes on the host whose $-IP$ is always much lower than that of the nearby guest.

It is clear that the hole transfer is the only downhill process to transfer charge from host to the neutral guest, we therefore consider the electron transfer from host to the guest cation. In Figure 7, owing to the existence of the hole on the guest, the electron energies of the guest and the nearby host both become lower. Furthermore, the guest $-EA$ lowers more than the host, causing the guest electron levels to be below the host electron levels. As a result, the

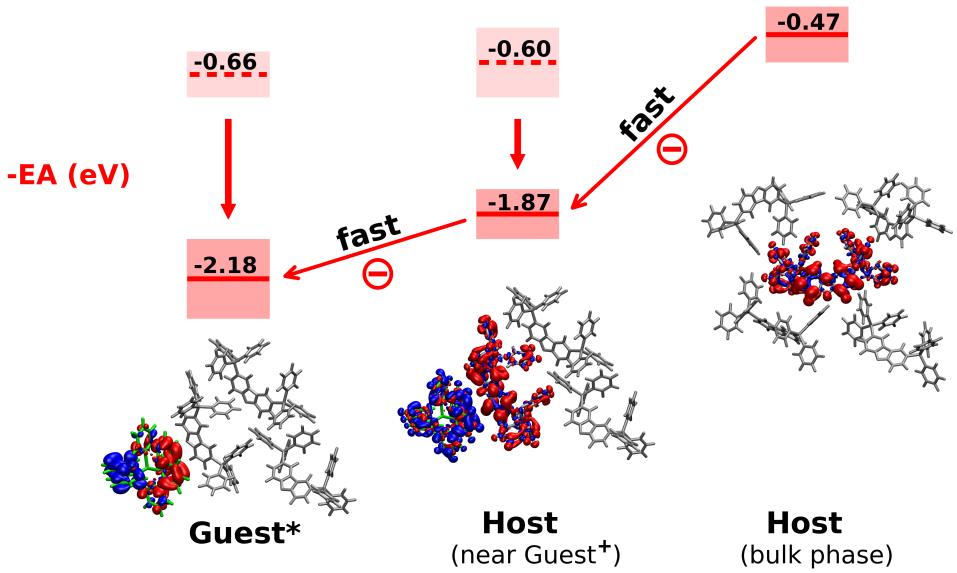

Figure 7: Charge recombination on the guest through electron transfer to the guest cation. The standard deviations are shown by the red regions around the energy levels.

electrons would not be trapped by the host and can recombine with the holes on the guest quickly.

For this specific host-guest system, we find one possible charge recombination mechanism to be the direct charge trapping. This finding could be significant for designing efficient host-guest systems. If this meachanism is dominant in a host-guest system, fast and well-balanced charge transfers should be the topmost consideration in experiments. Taking our system as an example, the electron energy of the host should be high enough in order to make the direct electron transfer as fast as the hole transfer. In addition, although the large offset between host and guest IPs gives fast hole transfer, it may create a narrow recombination zone in the emission layer which is far away from the electron transport side. As a result, this imbalance of hole and electron transfer would cause the degradation of OLED devices.[61] Thus, to make the offset of energy levels appropriate is also helpful. However, we also note that this mechanism may not be universal in all host-guest systems. One needs to do analysis on more host-guest combinations to gain a comprehensive understanding.

Conclusions and Future Work

In this article, we investigate the charge recombination in a model PhOLED host-guest system consisting of $Ir(ppy)_3$ and BTDF employing the QM/MM technique. Using IPs and EAs of the guest and host from QM/MM calculations, we introduce a new reaction coordinate to account for the influence of the guest on the energetics of the host, which is also correlated with the distance between them. We show that the larger host-guest interaction results in broader distributions of the host IP and EA. Then we describe a molecular picture of charge recombination on the guest through a charge trapping route: holes are transferred to the guest first, after which the electrons are attracted by the holes to form excitons on the guest.

This work could help the rational design of OLED host-guest systems. The results for the $Ir(ppy)_3$/BTDF system suggest that consideration of the energy level change in a host-guest mixture environment is needed to gain more accurate insight into the energy level alignment. Meanwhile, to design fast well-balanced charge trapping routes for host-guest systems may be critical for improving the device efficiency.

For future studies, we would like to investigate more PhOLED host-guest systems using the technique developed in this work. Different charge recombination routes are expected to be found for different combinations. Besides, we plan to study the energy transfer between the host and the guest in order to better understand charge recombination mechanisms. Additionally, we also want to study the host-guest systems for a newly developed type of OLED—Thermally Activated Delayed Fluorescence (TADF) OLED,[62–64] which is also proven to be highly efficient by harvesting both singlet and triplet excitons to generate fluorescence. Through such investigation, we hope to help better design the host-guest systems in new types of OLED devices.

Acknowledgement

We thank Dr. Denis Andrienko for the BTDF force field. T. Z. thanks Dr. Shuhao Wen,

Dr. David McMahon and Dr. Piotr de Silva for helpful discussions. This work was funded by a grant from Samsung (No.692030). T. V. is a David and Lucile Packard Foundation Fellow.

Supporting Information Available

Tests of basis set and density functional effects on IP/EA values, another version of Figures 3-4, MD parameters and the DFT calculation of the polarizabilities and dipole moments of the guest and host. This material is available free of charge via the Internet at `http://pubs.acs.org/`.

References

(1) Tang, C. W.; VanSlyke, S. A. Organic Electroluminescent Diodes. *Appl. Phys. Lett.* **1987**, *51*, 913–915.

(2) Baldo, M. A.; O'brien, D.; You, Y.; Shoustikov, A.; Sibley, S.; Thompson, M.; Forrest, S. Highly Efficient Phosphorescent Emission from Organic Electroluminescent Devices. *Nature* **1998**, *395*, 151–154.

(3) Baldo, M. A.; Lamansky, S.; Burrows, P.; Thompson, M.; Forrest, S. Very High-efficiency Green Organic Light-Emitting Devices Based on Electrophosphorescence. *Appl. Phys. Lett.* **1999**, *75*, 4.

(4) Adachi, C.; Baldo, M. A.; Forrest, S. R.; Thompson, M. E. High-efficiency Organic Electrophosphorescent Devices with Tris (2-phenylpyridine) iridium Doped into Electron-transporting Materials. *Appl. Phys. Lett.* **2000**, *77*, 904.

(5) Sun, Y.; Giebink, N. C.; Kanno, H.; Ma, B.; Thompson, M. E.; Forrest, S. R. Man-

agement of Singlet and Triplet Excitons for Efficient White Organic Light-Emitting Devices. *Nature* **2006**, *440*, 908–912.

(6) Reineke, S.; Lindner, F.; Schwartz, G.; Seidler, N.; Walzer, K.; Lüssem, B.; Leo, K. White Organic Light-Emitting Diodes with Fluorescent Tube Efficiency. *Nature* **2009**, *459*, 234–238.

(7) Tessler, N.; Denton, G.; Friend, R. Lasing from Conjugated-polymer Microcavities. *Nature* **1996**, *382*, 695–697.

(8) Lamansky, S.; Djurovich, P.; Murphy, D.; Abdel-Razzaq, F.; Lee, H.-E.; Adachi, C.; Burrows, P. E.; Forrest, S. R.; Thompson, M. E. Highly Phosphorescent Bis-cyclometalated Iridium Complexes: Synthesis, Photophysical Characterization, and Use in Organic Light Emitting Diodes. *J. Am. Chem. Soc.* **2001**, *123*, 4304–4312.

(9) Uoyama, H.; Goushi, K.; Shizu, K.; Nomura, H.; Adachi, C. Highly Efficient Organic Light-Emitting Diodes from Delayed Fluorescence. *Nature* **2012**, *492*, 234–238.

(10) Tanaka, D.; Sasabe, H.; Li, Y.-J.; Su, S.-J.; Takeda, T.; Kido, J. Ultra High Efficiency Green Organic Light-Emitting Devices. *Jpn. J. Appl. Phys.* **2007**, *46*, L10.

(11) Su, S.-J.; Cai, C.; Kido, J. RGB Phosphorescent Organic Light-Emitting Diodes by Using Host Materials with Heterocyclic Cores: Effect of Nitrogen Atom Orientations. *Chem. Mater.* **2010**, *23*, 274–284.

(12) Jeon, S. O.; Jang, S. E.; Son, H. S.; Lee, J. Y. External Quantum Efficiency Above 20% in Deep Blue Phosphorescent Organic Light-Emitting Diodes. *Adv. Mater.* **2011**, *23*, 1436–1441.

(13) Tao, Y.; Wang, Q.; Ao, L.; Zhong, C.; Qin, J.; Yang, C.; Ma, D. Molecular Design of Host Materials Based on Triphenylamine/Oxadiazole Hybrids for Excellent Deep-red Phosphorescent Organic Light-Emitting Diodes. *J. Mater. Chem.* **2010**, *20*, 1759–1765.

(14) Brown, A.; Pichler, K.; Greenham, N.; Bradley, D.; Friend, R. H.; Holmes, A. Optical Spectroscopy of Triplet Excitons and Charged Excitations in Poly (p-phenylenevinylene) Light-Emitting Diodes. *Chem. Phys. Lett.* **1993**, *210*, 61–66.

(15) Baldo, M.; O'brien, D.; Thompson, M.; Forrest, S. Excitonic Singlet-triplet Ratio in a Semiconducting Organic Thin Film. *Phys. Rev. B* **1999**, *60*, 14422.

(16) Cleave, V.; Yahioglu, G.; Barny, P. L.; Friend, R. H.; Tessler, N. Harvesting Singlet and Triplet Energy in Polymer LEDs. *Adv. Mater.* **1999**, *11*, 285–288.

(17) Yersin, H. *Transition Metal and Rare Earth Compounds*; Springer, 2004; pp 1–26.

(18) Adachi, C.; Baldo, M. A.; Thompson, M. E.; Forrest, S. R. Nearly 100% Internal Phosphorescence Efficiency in an Organic Light-Emitting Device. *J. Appl. Phys* **2001**, *90*, 5048–5051.

(19) Williams, E. L.; Haavisto, K.; Li, J.; Jabbour, G. E. Excimer-based White Phosphorescent Organic Light-Emitting Diodes with Nearly 100% Internal Quantum Efficiency. *Adv. Mater.* **2007**, *19*, 197–202.

(20) Xiao, L.; Su, S.-J.; Agata, Y.; Lan, H.; Kido, J. Nearly 100% Internal Quantum Efficiency in an Organic Blue-Light Electrophosphorescent Device Using a Weak Electron Transporting Material with a Wide Energy Gap. *Adv. Mater.* **2009**, *21*, 1271–1274.

(21) Tsai, M.-H.; Lin, H.-W.; Su, H.-C.; Ke, T.-H.; Wu, C.-C.; Fang, F.-C.; Liao, Y.-L.; Wong, K.-T.; Wu, C.-I. Highly Efficient Organic Blue Electrophosphorescent Devices Based on 3, 6-Bis (triphenylsilyl) carbazole as the Host Material. *Adv. Mater.* **2006**, *18*, 1216–1220.

(22) Tao, Y.; Yang, C.; Qin, J. Organic Host Materials for Phosphorescent Organic Light-Emitting Diodes. *Chem. Soc. Rev.* **2011**, *40*, 2943–2970.

(23) Chaskar, A.; Chen, H.-F.; Wong, K.-T. Bipolar Host Materials: A Chemical Approach for Highly Efficient Electrophosphorescent Devices. *Adv. Mater.* **2011**, *23*, 3876–3895.

(24) Yeh, S.-J.; Wu, M.-F.; Chen, C.-T.; Song, Y.-H.; Chi, Y.; Ho, M.-H.; Hsu, S.-F.; Chen, C. H. New Dopant and Host Materials for Blue-Light-Emitting Phosphorescent Organic Electroluminescent Devices. *Adv. Mater.* **2005**, *17*, 285–+.

(25) Tokito, S.; Iijima, T.; Suzuri, Y.; Kita, H.; Tsuzuki, T.; Sato, F. Confinement of Triplet Energy on Phosphorescent Molecules for Highly-efficient Organic Blue-Light-Emitting Devices. *Appl. Phys. Lett.* **2003**, *83*, 569–571.

(26) Shih, P.-I.; Chien, C.-H.; Wu, F.-I.; Shu, C.-F. A Novel Fluorene-Triphenylamine Hybrid that is a Highly Efficient Host Material for Blue-, Green-, and Red-Light-Emitting Electrophosphorescent Devices. *Adv. Funct. Mater.* **2007**, *17*, 3514–3520.

(27) Vecchi, P. A.; Padmaperuma, A. B.; Qiao, H.; Sapochak, L. S.; Burrows, P. E. A Dibenzofuran-based Host Material for Blue Electrophosphorescence. *Org. Lett.* **2006**, *8*, 4211–4214.

(28) Son, H. S.; Seo, C. W.; Lee, J. Y. Correlation of the Substitution Position of Diphenylphosphine Oxide on Phenylcarbazole and Device Performances of Blue Phosphorescent Organic Light-Emitting Diodes. *J. Mater. Chem.* **2011**, *21*, 5638–5644.

(29) Suzuki, H.; Hoshino, S. Effects of Doping Dyes on the Electroluminescent Characteristics of Multilayer Organic Light-Emitting Diodes. *J. Appl. Phys* **1996**, *79*, 8816–8822.

(30) Nüesch, F.; Berner, D.; Tutiš, E.; Schaer, M.; Ma, C.; Wang, X.; Zhang, B.; Zuppiroli, L. Doping-induced Charge Trapping in Organic Light-Emitting Devices. *Adv. Funct. Mater.* **2005**, *15*, 323–330.

(31) Förster, T. Zwischenmolekulare Energiewanderung und Fluoreszenz. *Ann. Phys. (Berlin)* **1948**, *437*, 55–75.

(32) Dexter, D. L. A Theory of Sensitized Luminescence in Solids. *J. Chem. Phys.* **1953**, *21*, 836–850.

(33) Förster, T. 10th Spiers Memorial Lecture. Transfer Mechanisms of Electronic Excitation. *Disc. Faraday Soc.* **1959**, *27*, 7–17.

(34) Cho, Y. J.; Yook, K. S.; Lee, J. Y. A Universal Host Material for High External Quantum Efficiency Close to 25% and Long Lifetime in Green Fluorescent and Phosphorescent OLEDs. *Adv. Mater.* **2014**, *26*, 4050–4055.

(35) Chou, H.-H.; Cheng, C.-H. A Highly Efficient Universal Bipolar Host for Blue, Green, and Red Phosphorescent OLEDs. *Adv. Mater.* **2010**, *22*, 2468–2471.

(36) May, F.; Al-Helwi, M.; Baumeier, B.; Kowalsky, W.; Fuchs, E.; Lennartz, C.; Andrienko, D. Design Rules for Charge-transport Efficient Host Materials for Phosphorescent Organic Light-Emitting Diodes. *J. Am. Chem. Soc.* **2012**, *134*, 13818–13822.

(37) May, F.; Baumeier, B.; Lennartz, C.; Andrienko, D. Can Lattice Models Predict the Density of States of Amorphous Organic Semiconductors? *Phys. Rev. Lett.* **2012**, *109*, 136401.

(38) Kordt, P.; van der Holst, J. J.; Al Helwi, M.; Kowalsky, W.; May, F.; Badinski, A.; Lennartz, C.; Andrienko, D. Modeling of Organic Light Emitting Diodes: From Molecular to Device Properties. *Adv. Funct. Mater.* **2015**, *25*, 1955–1971.

(39) Pelzer, K. M.; Darling, S. B. Charge Generation in Organic Photovoltaics: A Review of Theory and Computation. *Mol. Syst. Des. & Eng.* **2016**, *1*, 10–24.

(40) Brédas, J.-L.; Norton, J. E.; Cornil, J.; Coropceanu, V. Molecular Understanding of Organic Solar Cells: the Challenges. *Acc. Chem. Res.* **2009**, *42*, 1691–1699.

(41) Åqvist, J.; Warshel, A. Simulation of Enzyme Reactions Using Valence Bond Force

Fields and Other Hybrid Quantum/Classical Approaches. *Chem. Rev.* **1993**, *93*, 2523–2544.

(42) Difley, S.; Wang, L.-P.; Yeganeh, S.; Yost, S. R.; Van Voorhis, T. Electronic Properties of Disordered Organic Semiconductors via QM/MM Simulations. *Acc. Chem. Res.* **2010**, *43*, 995–1004.

(43) Yost, S. R.; Wang, L.-P.; Van Voorhis, T. Molecular Insight into the Energy Levels at the Organic Donor/Acceptor Interface: A Quantum Mechanics/Molecular Mechanics Study. *J. Phys. Chem. C* **2011**, *115*, 14431–14436.

(44) Martínez, L.; Andrade, R.; Birgin, E. G.; Martínez, J. M. PACKMOL: A Package for Building Initial Configurations for Molecular Dynamics Simulations. *J. Comput. Chem.* **2009**, *30*, 2157–2164.

(45) Hess, B.; Kutzner, C.; Van Der Spoel, D.; Lindahl, E. GROMACS 4: Algorithms for Highly Efficient, Load-balanced, and Scalable Molecular Simulation. *J. Chem. Theory Comput.* **2008**, *4*, 435–447.

(46) Jorgensen, W. L.; Maxwell, D. S.; Tirado-Rives, J. Development and Testing of the OPLS All-atom Force Field on Conformational Energetics and Properties of Organic Liquids. *J. Am. Chem. Soc.* **1996**, *118*, 11225–11236.

(47) Brooks, B. R.; Bruccoleri, R. E.; Olafson, B. D.; States, D. J.; Swaminathan, S.; Karplus, M. CHARMM: A Program for Macromolecular Energy, Minimization, and Dynamics Calculations. *J. Comput. Chem.* **1983**, *4*, 187–217.

(48) Shao, Y.; Gan, Z.; Epifanovsky, E.; Gilbert, A. T. B.; Wormit, M.; Kussmann, J.; Lange, A. W.; Behn, A.; Deng, J.; Feng, X. et al. Advances in Molecular Quantum Chemistry Contained in the Q-Chem 4 Program Package. *Mol. Phys.* **2015**, *113*, 184–215.

(49) Woodcock, H. L.; Hodošček, M.; Gilbert, A. T.; Gill, P. M.; Schaefer, H. F.; Brooks, B. R. Interfacing Q-Chem and CHARMM to Perform QM/MM Reaction Path Calculations. *J. Comput. Chem.* **2007**, *28*, 1485–1502.

(50) Adamo, C.; Scuseria, G. E.; Barone, V. Accurate Excitation Energies from Time-dependent Density Functional Theory: Assessing the PBE0 Model. *J. Chem. Phys.* **1999**, *111*, 2889–2899.

(51) Hariharan, P. C.; Pople, J. A. The Influence of Polarization Functions on Molecular Orbital Hydrogenation Energies. *Theor. Chim. Acta.* **1973**, *28*, 213–222.

(52) Hay, P. J.; Wadt, W. R. Ab Initio Effective Core Potentials for Molecular Calculations. Potentials for K to Au Including the Outermost Core Orbitals. *J. Chem. Phys.* **1985**, *82*, 299–310.

(53) Kowalczyk, T.; Tsuchimochi, T.; Chen, P.-T.; Top, L.; Van Voorhis, T. Excitation Energies and Stokes Shifts from a Restricted Open-shell Kohn-Sham Approach. *J. Chem. Phys.* **2013**, *138*, 164101.

(54) Lamoureux, G.; Roux, B. Modeling Induced Polarization with Classical Drude Oscillators: Theory and Molecular Dynamics Simulation Algorithm. *J. Chem. Phys.* **2003**, *119*, 3025–3039.

(55) Hill, I.; Kahn, A.; Soos, Z.; Pascal Jr, R. Charge-separation Energy in Films of π-conjugated Organic Molecules. *Chem. Phys. Lett.* **2000**, *327*, 181–188.

(56) Krause, S.; Casu, M.; Schöll, A.; Umbach, E. Determination of Transport Levels of Organic Semiconductors by UPS and IPS. *New J. Phys.* **2008**, *10*, 085001.

(57) Rosenblatt, M. Remarks on Some Nonparametric Estimates of a Density Function. *Ann. Math. Stat.* **1956**, *27*, 832–837.

(58) Parzen, E. On Estimation of a Probability Density Function and Mode. *Ann. Math. Stat.* **1962**, *33*, 1065–1076.

(59) D'Andrade, B. W.; Datta, S.; Forrest, S. R.; Djurovich, P.; Polikarpov, E.; Thompson, M. E. Relationship between the Ionization and Oxidation Potentials of Molecular Organic Semiconductors. *Org. Electron.* **2005**, *6*, 11–20.

(60) Yoshida, H.; Yoshizaki, K. Electron Affinities of Organic Materials Used for Organic Light-Emitting Diodes: A Low-energy Inverse Photoemission Study. *Org. Electron.* **2015**, *20*, 24–30.

(61) Scholz, S.; Kondakov, D.; LuÌĹssem, B.; Leo, K. Degradation Mechanisms and Reactions in Organic Light-Emitting Devices. *Chem. Rev.* **2015**, *115*, 8449–8503.

(62) Uoyama, H.; Goushi, K.; Shizu, K.; Nomura, H.; Adachi, C. Highly Efficient Organic Light-Emitting Diodes from Delayed Fluorescence. *Nature* **2012**, *492*, 234–238.

(63) Sato, K.; Shizu, K.; Yoshimura, K.; Kawada, A.; Miyazaki, H.; Adachi, C. Organic Luminescent Molecule with Energetically Equivalent Singlet and Triplet Excited States for Organic Light-Emitting Diodes. *Phys. Rev. Lett.* **2013**, *110*, 247401.

(64) Nakanotani, H.; Masui, K.; Nishide, J.; Shibata, T.; Adachi, C. Promising Operational Stability of High-efficiency Organic Light-Emitting Diodes Based on Thermally Activated Delayed Fluorescence. *Sci. Rep.* **2013**, *3*, 2127–2132.

Graphical TOC Entry